Mesostructures

Random-Graft Polymer-Directed Synthesis of Inorganic Mesostructures with Ultrathin Frameworks**

Changbum Jo, Yongbeom Seo, Kanghee Cho, Jaeheon Kim, Hye Sun Shin, Munhee Lee, Jeong-Chul Kim, Sang Ouk Kim, Jeong Yong Lee, Hyotcherl Ihee, and Ryong Ryoo

Abstract: A widely employed route for synthesizing meso-structured materials is the use of surfactant micelles or amphiphilic block copolymers as structure-directing agents. A versatile synthesis method is described for mesostructured materials composed of ultrathin inorganic frameworks using amorphous linear-chain polymers functionalized with a random distribution of side groups that can participate in inorganic crystallization. Tight binding of the side groups with inorganic species enforces strain in the polymer backbones, limiting the crystallization to the ultrathin micellar scale. This method is demonstrated for a variety of materials, such as hierarchically nanoporous zeolites, their aluminophosphate analogue, TiO$_2$ nanosheets of sub-nanometer thickness, and mesoporous TiO$_2$, SnO$_2$, and ZrO$_2$. This polymer-directed synthesis is expected to widen our accessibility to unexplored mesostructured materials in a simple and mass-producible manner.

Mesostructures are structures with length scales ranging from molecular to macroscopic dimensions. These structures are ubiquitous in nanoparticles, nanocomposites, and mesoporous materials. Mesostructured materials are used in numerous applications, including catalysis,[1] separation,[2] energy storage/conversion,[3] and biomedicine,[4] and they provide platforms for building nanostructured architectures.[5,6] The traditional route for synthesizing mesostruc-tured materials often utilizes self-assembled structures, such as surfactant micelles[7–9] or amphiphilic block copolymer assemblies[10,11] as structure-directing agents (SDAs). Molecular assemblies of the amphiphilic materials provide soft template structures that confine the inorganic material formation to the nanoscale. Nevertheless, those soft templates are generally assembled by weak intermolecular forces, such as hydrophobic or van der Waals interactions. The resultant weak assemblies can fail to confine crystal growths within their template boundaries, particularly in syntheses of mes-ostructured materials with crystalline frameworks.[12] More-over, this strategy often requires specialized surfactants that are not readily available, and are complicated and expensive to synthesize.

Herein, we report a synthetic route to mesoporous materials that are directed by random-graft amorphous polymers. Our method attains highly crystalline mesostruc-tures of various inorganic materials without requiring a complicated synthesis or self-assembly process of surfactants or block copolymers. Amorphous linear polymers are randomly functionalized with organic groups that can form tight bonding to inorganic species. Such polymers were able to direct the formation of highly crystalline inorganic meso-structures, including ultrathin nanosheets or a nanosponge. This random-graft polymer-directed synthesis offers a general route to various types of functional inorganic mesostructures, such as hierarchically nanoporous zeolites, their alumino-phosphate analogues (AlPO$_4$ and other related metal phos-phates with open frameworks), titanium dioxide (TiO$_2$) nanosheets of subnanometer thickness, and mesoporous TiO$_2$, SnO$_2$, and ZrO$_2$.

Zeolites belong to a family of crystalline microporous aluminosilicates that have been widely used as catalysts and adsorbents.[13,14] Zeolite with various structures has structural analogues composed of AlPO$_4$ instead of aluminosilicate. The incorporation of mesoporosity into these materials has been an important issue for resolving the diffusion limitation for bulky adsorbates.[15] Mesopore generation can be achieved using linear polystyrene functionalized with multi-ammonium SDA groups. Figure 1 shows the synthesis results for a zeolite with the structure type MFI, in which the SDA was a tri-ammonium group with the structural formula of $-N^+(CH_3)_2-C_6H_{12}-N^+(CH_3)_2-C_6H_{12}-N^+(CH_3)_2-C_6H_{13}$ (Figure 1a). This SDA group is denoted by "N$_3$-SDA". As demonstrated by scanning electron microscopy (SEM), thin MFI nanocrystals were connected into a nanosponge-like, three-dimensional network in this zeolite (Figure 1b). High-resolution trans-mission electron microscopy (TEM) indicated that the zeolite nanocrystals in the sponge were uniformly tailored to a thick-

[*] Dr. C. Jo, Dr. Y. Seo, Dr. K. Cho, J. Kim, H. S. Shin, M. Lee, J.-C. Kim, Prof. S. O. Kim, Prof. J. Y. Lee, Prof. H. Ihee, Prof. R. Ryoo
Center for Nanomaterials and Chemical Reactions
Institute for Basic Science (IBS)
Daejeon 305-701 (Republic of Korea)

J. Kim, H. S. Shin, M. Lee, Prof. H. Ihee, Prof. R. Ryoo
Department of Chemistry, KAIST
Daejeon 305-701 (Republic of Korea)
E-mail: rryoo@kaist.ac.kr
Homepage: http://rryoo.kaist.ac.kr

J.-C. Kim
Graduate School of Nanoscience and Technology, KAIST
Daejeon 305-701 (Republic of Korea)

Prof. S. O. Kim, Prof. J. Y. Lee
Department of Materials Science and Engineering, KAIST
Daejeon 305-701 (Republic of Korea)
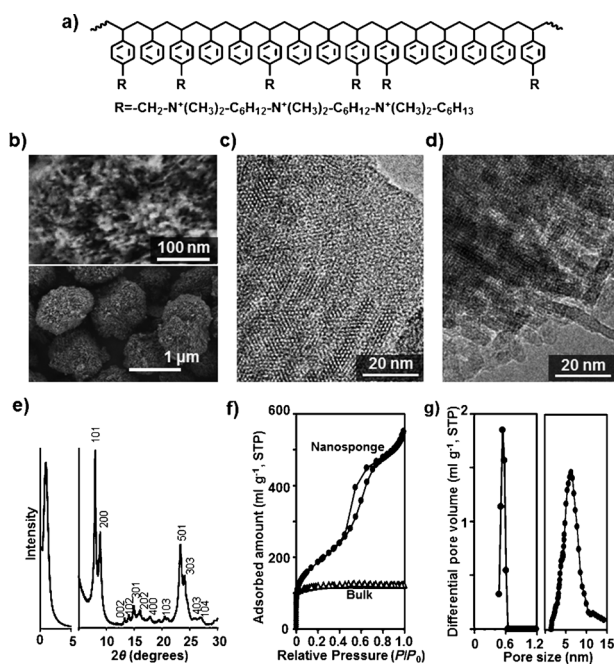
Figure 1. Random-graft polymer-directed synthesis of zeolite nano-sponges. a) Molecular structure of the polymer used in MFI zeolite synthesis. b), c) SEM and TEM images of the as-synthesized MFI zeolite nanosponge. d), e) TEM image and XRD pattern of the MFI zeolite after removal of the polymer by calcination. f) Argon sorption isotherm of the calcined MFI zeolite at 87 K, in comparison with bulk MFI. g) Pore-size distribution derived from the adsorption isotherm, using NLDFT.

ness of 4.5 nm along the crystal *b*-axis (Figure 1 c). The lateral size of each crystal domain was less than 20 nm (Supporting Information, Section S1). The zeolite exhibited powder X-ray diffraction (XRD) peaks corresponding to the MFI crystal structure, except that the reflections along the *b*-axis were absent owing to the nanosheet-type mesostructure (Figure 1 e).[16] The mesostructured zeolite was collected as a composite material with polymers. In the as-synthesized state, the zeolite exhibited no micro or mesoporosity, which indicated that the micropores in the zeolite domain were occupied by SDA groups. The space between the zeolite domains was filled with polymers. An elemental analysis of the zeolite-polymer composite yielded an N/SiO_2 molar ratio equal to 0.12, which is twice the SDA content that could exist in the zeolite micropores. This analysis indicated that approximately 50% of the N_3-SDA groups acted as the zeolite SDA, while the remainder existed as bystanders in the polymer region. Similar results showing a nanosponge-type mesostructure were obtained from the syntheses of beta zeolite and $AlPO_4$ with structure type ATO (Supporting Information, Section S2). The beta zeolite nanosponge was synthesized using polystyrene grafted with tetraammonium containing two piperidinium groups (see the Supporting Information, Section S2 for its molecular structure), whereas for the $AlPO_4$ nanosponge, polystyrene was functionalized with the same N_3-SDA used for MFI zeolite. The incorporation of the SDA groups within the $AlPO_4$ framework was confirmed by ^{31}P–^1H two-dimensional heteronuclear correla-

tion NMR spectroscopy (Supporting Information, Section S3).

The mesopores and micropores in the zeolite nanosponge (and also $AlPO_4$) can be opened by calcination treatment in air, which decomposes the polymers. A TEM image of the calcined samples revealed the retention of nanosponge-type mesostructures after calcination (Figure 1 d). The calcined zeolite exhibited a well-resolved Bragg reflection peak centered at $2\theta = 0.87°$ in the XRD pattern (Figure 1 e). This peak indicated that there should be significant short-range structural ordering in the zeolite nanosponge. For a disordered mesostructure, this kind of structure coherence only occurs when uniform mesopores are retained between zeolite frameworks of uniform thickness. An analysis of these mesopores with nonlocal density functional theory (NLDFT) using the argon adsorption isotherm indicated a very sharp distribution of diameters centered at 6.4 nm (Figure 1 g). This zeolite is the first example of direct synthesis using molecular SDAs for pure MFI zeolite self-supporting uniform mesopores.[17,18] Furthermore, we can systematically control the mesopore diameters according to the degree of SDA functionalization along the polymer chains. The mode diameter increased from 2.7 to 11 nm as the functionalization degree decreased from 80% to 20% of a styrene unit (Supporting Information, Section S4). This relationship can be explained by the increase in the polymer portion compared to the zeolite crystal domain. However, zeolite did not form below 10% functionalization. With such low functionalization, sparsely distributed SDA groups inhibit the formation of micelles owing to the need for excessive polymer strain or steric hindrance. Based on this simple principle, it is possible to synthesize zeolites with tailored mesopores. The zeolites are promising as strong solid acids that can support transition-metal nanoparticles within the uniform mesopores for applications as bifunctional catalysts. For example, MFI zeolite nanosponge supporting cobalt nanoparticles exhibited remarkably high resistance to metal agglomeration during catalytic application in Fischer–Tropsch synthesis (Supporting Information, Section S5). Consequently, the catalyst displayed much better catalytic performance (high conversion of CO, high selectivity to branched hydrocarbons in the gasoline range) than conventional MFI zeolite.

Based on the zeolites and $AlPO_4$ synthesis, a random-graft polymer-directed mechanism is proposed (Figure 2). In this mechanism, amorphous linear polymers are functionalized with side groups that have a strong chemical affinity to a precursor of inorganic crystal. The functionalization is conducted at random intervals along the polymer backbone. The polymer molecules are dissolved in water or an organic solvent. When an inorganic precursor is added to this solution, the functional groups bind with the inorganic species. As a result, the inorganic species becomes highly concentrated along the polymer chains, causing polymerization of the inorganic species to form a mesostructured gel. Subsequently, the inorganic part is transformed to a crystalline framework. In the case of zeolite and $AlPO_4$, the electrostatic force binds the negatively charged inorganic species and positively charged ammonium groups. This electrostatic
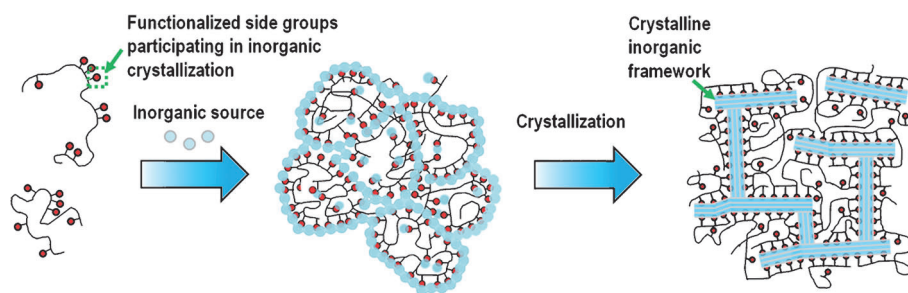
Figure 2. Description of random-graft polymer-directed inorganic crystallization. Amorphous linear polymers are functionalized with inorganic structure-directing side groups. An inorganic precursor with tight binding to the polymer groups is added into a solution containing the polymers. The binding of inorganic species to polymer side groups leads to an increase in inorganic concentration along the polymer chain, which promotes polymerization of inorganic species to form a mesostructured polymer–inorganic composite gel. Upon subsequent solvothermal treatment, the inorganic is transformed to a crystalline framework while tight bonding to polymer is maintained. As the crystal starts to grow, polymer backbones become crowded around surfaces of inorganic crystals. The steric hindrance by the polymer restricts the crystal growths to a thickness of only a few nanometers.

binding is necessary for the ammonium to function as an SDA for the consecutive conversion of the amorphous inorganic gel to the zeolite framework. The ammonium groups should have an adequate structure and size to function as an SDA for a particular type of microporous framework. The crystalline microporous framework is not generated without an adequate SDA. The ammonium group is embedded within the inorganic framework owing to the tight encasing of the framework. Under such circumstances, polymer chains remain rigidly bound to every crystallite surface. Further crystal growth leading to Oswald ripening is therefore suppressed. Although each functional group in a crystallite may come from a different polymer chain, it is more likely that multiple groups come from the same polymer chain. As the polymer chains are unable to penetrate the densely packed crystal structure, the polymer backbones become crowded around the surfaces of the inorganic crystal. Consequently, the polymer segments near the surfaces lead to steric hindrance, which then limits crystal growth to a micelle-like region of only a few nanometers thickness. Evidence for this mechanism can be obtained by a structure analysis along the reaction time line for the example of MFI zeolite nanosponge, using XRD, solid state ^{29}Si NMR spectroscopy, SEM, and TEM (Supporting Information, Section S6). The present polymer-directed synthesis approach has significant advantages for synthesizing uniformly mesoporous materials built with open microporous frameworks of various compositions. Examples are aluminosilicate zeolites, silica, $AlPO_4$, silicoaluminophosphates known as SAPOs, cobalt–zinc phosphates, and chalcogenides. Many of these are synthesized by structure-directing amines or ammonium species.[19]

The present strategy can be extended to the synthesis of non-microporous inorganic oxides, such as TiO_2, SnO_2, and ZrO_2, if the polymer–inorganic pairs are rationally chosen to maintain tight binding between the polymer groups and the oxide surfaces. Unlike the aforementioned open frameworks, however, these non-porous oxide frameworks cannot encase polymer groups. Simple electrostatic interactions are not sufficient for generating highly mesoporous morphologies.

For example, consider an aqueous solution in which polymers with anionic groups (for example, poly(styrene sulfonate)) are dissolved with $TiOCl_2$. Here, the polymer groups are not an essential SDA for the formation of TiO_2. Thus, the TiO_2 can be precipitated by adjusting the pH of the solution with a base, regardless of the presence of the polymer. The presence of the polymers can cause the TiO_2 crystal size to decrease conspicuously, whereas the polymer $-SO_3^-$ groups inhibit crystal growth by surface adsorption.[20] However, the polymer binding is much less effective compared to the aforementioned synthesis of zeolite and $AlPO_4$ frameworks. This can be attributed to chloride ions that replace the polymer groups from the TiO_2 crystal surfaces during the oxide nucleation and subsequent growth. Such an excessive crystal growth is a common problem occurring during the synthesis of mesoporous materials using surfactant micelles or water-soluble block copolymers with ionic precursors. Thus, non-aqueous solvothermal synthesis is desirable. A polymer–inorganic pair with covalent or coordination bonding has a distinct advantage over electrostatic interaction.[11] Suitable polymer–inorganic pairs for the synthesis of TiO_2, SnO_2, and ZrO_2 can be selected according to this guideline.

Figure 3 shows the solvothermal synthesis results for TiO_2 (titania) employing polymer–inorganic pairs with covalent or coordination bonding. The solvothermal synthesis was performed with two different polymers dissolved in dimethylformamide: poly(acrylic acid) and poly(4-vinylphenol-*co*-methyl methacrylate). Titanium *iso*-propoxide was selected as the TiO_2 precursor when poly(acrylic acid) was used, whereas the $-COOH$ groups bound the TiO_2 precursor through coordination bonding.[21] $TiCl_4$ was selected as the TiO_2 precursor instead of titanium *iso*-propoxide when poly(4-vinylphenol-*co*-methyl methacrylate) was used. In this latter case, the phenol groups formed phenol O$-$Ti covalent bonding by the reaction with $TiCl_4$.[22] This led to the generation of mesostructured TiO_2 according to Figure 2, which was confirmed by investigation using XRD, TEM, and FTIR spectroscopy (Supporting Information, Section S7). Both polymers yielded almost indistinguishable results (Figure 3a,b). A disordered assembly of ultrathin TiO_2 nanosheets with 0.7 nm thickness was obtained at a low molar ratio of Ti/functional group in both polymers (Figure 3a). The nanosheets possessed an anatase structure with dominant (010) surfaces.[23,24] When the Ti/functional group ratio was increased, both polymers yielded TiO_2 nanosponges that were irregularly composed of approximately 3 nm thick anatase frameworks (Figure 3b). The nanosponge exhibited a broad small-angle XRD peak centered at $2\theta = 1.2°$, along with to wide-angle peaks indicating an anatase structure (Figure 3c). The appearance of the small-angle peak indicated significant short-range structural
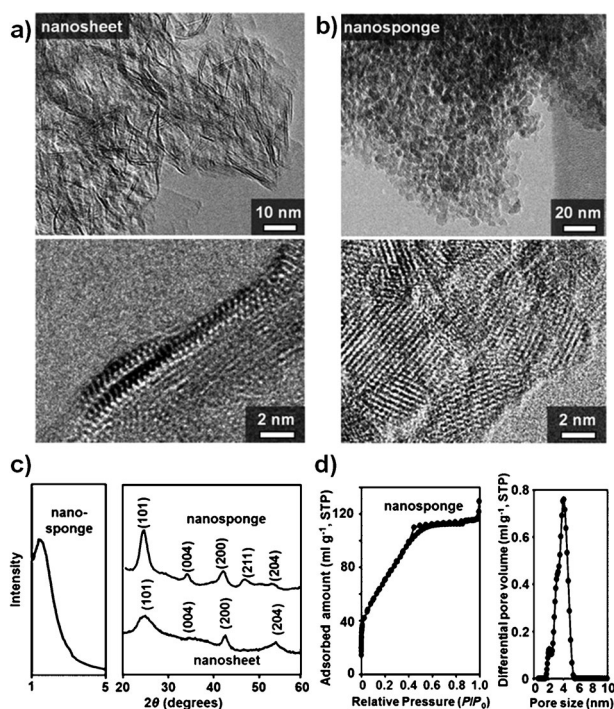
Figure 3. Polymer-directed synthesis of TiO$_2$ nanosheets and nanosponge. a), b) TEM images; c) XRD patterns; d) nitrogen adsorption–desorption isotherms at 77 K, and the corresponding pore-size distribution derived by NLDFT analysis.

ordering, similar to the zeolite nanosponge shown in Figure 1. Both the TiO$_2$ nanosheet and the nanosponge were stable under calcination treatment in air at 623 K, so that the space between the nanocrystalline TiO$_2$ frameworks could be safely open. The TiO$_2$ nanosponge exhibited a type IV nitrogen adsorption–desorption isotherm, from which the NLDFT analysis gave a very narrow distribution of mesopore diameters centered at 4.0 nm (Figure 3 d). The specific surface area of the nanosponge measured by the BET method was 270 m^{2}g^{-1}. The BET area of the nanosheet was 350 m^{2}g^{-1}. This is remarkable as a TiO$_2$ with crystalline framework (Supporting Information, Section S7). Crystalline TiO$_2$ with a high specific surface area with dominant high-energy facets is desirable in photocatalytic applications.[25] TiO$_2$ is one of the most important inorganic crystals currently attracting scientific attention, owing to its applications in low-cost, high-efficiency solar cells, photochemical catalysts, lithium batteries, and catalyst supports with strong metal interactions.[26,27] The efficiencies of TiO$_2$ in these applications and resulting future technological advances depend on the synthesis of ultrathin nanocrystalline TiO$_2$ with a high specific surface area and a large intercrystalline mesopore volume. Along with TiO$_2$, this polymer-directed synthesis was also effective for SnO$_2$ and ZrO$_2$ nanosponges (Supporting Information, Section S8).

In conclusion, we demonstrated the generation of mesostructured inorganic materials through polymer-directed synthesis, for a number of representative examples, such as mesoporous MFI zeolites, mesoporous AlPO$_4$ with ATO-type framework, TiO$_2$ nanosheets, SnO$_2$ and TiO$_2$ nanosponges,

and mesoporous ZrO$_2$. In the MFI zeolite, TiO$_2$, and SnO$_2$ nanosponges, there was even a short-range ordering between nearest-neighboring frameworks that constituted the mesoporous sponges. The used polymers were not amphiphilic block copolymers, but were amorphous, random-coil, linear-chain polymers grafted with appropriate SDA groups. It was possible to choose polymer–inorganic pairs that could maintain tight bonding during the course of the mesostructure formation. The tight bonding provides a simple guideline for the choice of polymer–inorganic pairs. Many mass-produced polymers can be readily functionalized, and the functionalization can be performed at random intervals along the chains. The functional group density can be used to control mesostructural parameters, such as the nanosheet widths and mesopore diameters. Overall, the polymer-directed synthesis may permit access to the unexplored realm of inorganic materials and polymer–inorganic composites with various chemical compositions and mesostructures.

Experimental Section

The synthesis details for polymers and mesostructured inorganic materials are provided in Supporting Information. A random copolymer of styrene and 4-chloromethylstyrene was synthesized by nitroxide-mediated radical polymerization. Forty molar percent of 4-chloromethylstyrene relative to the total number of moles of the monomers was used for polymerization. The molecular weight and polydispersity index of the resultant polymer were 75 000 g mol^{-1} and 2.3, respectively. Irregularly spaced chloromethyl side groups in copolymer chains were reacted with equimolar amounts of N(Me)$_2$–C$_6$H$_{12}$–N(Me)$_2$$^+$–C$_6H_{12}$–N(Me)$_2$$^+$–C$_6H_{13}$ in dimethylformamide. The mixture was heated in an oil bath at 323 K for 1 d with vigorous stirring. After cooling to room temperature, the product was precipitated with diethyl ether, filtered, and dried in a vacuum oven at 303 K for 12 h. The precipitated polymers were used as MFI zeolite SDAs. In a typical synthesis of polymer-MFI zeolite mesostructure, sodium silicate solution (26.5 % SiO$_2$, 10.6 % Na$_2$O, Sigma–Aldrich), Al$_2$SO$_4$·18H$_2$O (98 %, Sigma–Aldrich), sulfuric acid (47 % H$_2$SO$_4$, Wako), and the synthesized amorphous polymer were mixed with distilled water to obtain a gel composition of 100 SiO$_2$: 1 Al$_2$O$_3$: 39 Na$_2$O: 27 H$_2$SO$_4$: 400 ethanol: 0.37 polymer: 6000 H$_2$O. The mixed gel was stirred at 333 K for 12 h and then transferred to a Teflon-coated stainless-steel autoclave. The autoclave was heated at 423 K for 6.5 d while tumbling. After the hydrothermal treatment, the zeolite-polymer composite was filtered, washed with distilled water and dried in a convection oven at 373 K. The product was calcined at 853 K for 4 h under flowing air. No zeolite crystals were obtained under the same conditions without polymers, confirming that the amorphous polymer functioned as MFI zeolite SDAs.

[1] A. Corma, *Chem. Rev.* **1997**, *97*, 2373.
[2] K. Nakanishi, N. Tanaka, *Acc. Chem. Res.* **2007**, *40*, 863.
[3] C. Vix-Guterl, E. Frackowiak, K. Jurewicz, M. Friebe, J. Parmentier, F. Béguin, *Carbon* **2005**, *43*, 1293.

[4] M. Vallet-Regí, F. Balas, D. Arcos, *Angew. Chem.* **2007**, *119*, 7692; *Angew. Chem. Int. Ed.* **2007**, *46*, 7548.

[5] S. H. Joo, S. J. Choi, I. Oh, J. Kwak, Z. Liu, O. Terasaki, R. Ryoo, *Nature* **2001**, *412*, 169.

[6] A.-H. Lu, F. Schüth, *Adv. Mater.* **2006**, *18*, 1793.

[7] C. T. Kresge, M. E. Leonowicz, W. J. Roth, J. C. Vartuli, J. S. Beck, *Nature* **1992**, *359*, 710.

[8] Q. Huo, D. I. Margolese, U. Ciesla, P. Feng, T. E. Gier, P. Sieger, R. Leon, P. M. Petroff, F. Schüth, G. D. Stucky, *Nature* **1994**, *368*, 317.

[9] C. G. Göltner, M. Antonietti, *Adv. Mater.* **1997**, *9*, 431.

[10] S. Förster, M. Antonietti, *Adv. Mater.* **1998**, *10*, 195.

[11] P. Yang, D. Zhao, D. I. Margolese, B. F. Chmelka, G. D. Stucky, *Nature* **1998**, *396*, 152.

[12] A. Karlsson, M. Stöcker, R. Schmidt, *Microporous Mesoporous Mater.* **1999**, *27*, 181.

[13] A. Corma, *J. Catal.* **2003**, *216*, 298.

[14] R. E. Morris, P. S. Wheatley, *Angew. Chem.* **2007**, *119*, 5044; *Angew. Chem. Int. Ed.* **2008**, *47*, 4966.

[15] J. Pérez-Ramírez, C. H. Christensen, K. Egeblad, C. H. Christensen, J. C. Groen, *Chem. Soc. Rev.* **2008**, *37*, 2530.

[16] M. Choi, K. Na, J. Kim, Y. Sakamoto, O. Terasaki, R. Ryoo, *Nature* **2009**, *461*, 246.

[17] X. Zhang, D. Liu, D. Xu, S. Asahina, K. A. Cychosz, K. V. Agrawal, Y. A. Wahedi, A. Bhan, S. A. Hashimi, O. Terasaki, M. Thommes, M. Tsapatsis, *Science* **2012**, *336*, 1684.

[18] K. Na, W. Park, Y. Seo, R. Ryoo, *Chem. Mater.* **2011**, *23*, 1273.

[19] P. Feng, X. Bu, N. Zheng, *Acc. Chem. Res.* **2005**, *38*, 293.

[20] G. Wegner, P. Baum, M. Müller, J. Norwig, K. Landfester, *Macromol. Symp.* **2001**, *175*, 349.

[21] S. Doeuff, M. Henry, C. Sanchez, J. Livage, *J. Non-Cryst. Solids* **1987**, *89*, 206.

[22] S. Xia, Z. Fu, B. Huang, J. Xu, Z. Fan, *J. Mol. Catal. A* **2012**, *355*, 161.

[23] T. Sasaki, M. Watanabe, H. Hashizume, H. Yamada, H. Nakazawa, *J. Am. Chem. Soc.* **1996**, *118*, 8329.

[24] B. Wu, G. Guo, N. Zheng, Z. Xie, G. D. Stucky, *J. Am. Chem. Soc.* **2008**, *130*, 17563.

[25] H. G. Yang, C. H. Sun, S. Z. Qiao, J. Zou, G. Liu, S. C. Smith, H. M. Cheng, G. Q. Lu, *Nature* **2008**, *453*, 638.

[26] X. Chen, S. S. Mao, *Chem. Rev.* **2007**, *107*, 2891.

[27] R. Ma, T. Sasaki, *Adv. Mater.* **2010**, *22*, 5082.